The all-seeing eye of resonant Auger electron spectroscopy: a study on aqueous solution using tender x-rays

Tsveta Miteva,[*,†] Nikolai V. Kryzhevoi,[‡] Nicolas Sisourat,[†] Christophe Nicolas,[¶] Wandared Pokapanich,[§] Thanit Saisopa,[‖] Prayoon Songsiriritthigul,[‖] Yuttakarn Rattanachai,[⊥] Andreas Dreuw,[#] Jan Wenzel,[#] Jérôme Palaudoux,[†] Gunnar Öhrwall,[@] Ralph Püttner,[△] Lorenz S. Cederbaum,[‡] Jean-Pascal Rueff,[†,¶] and Denis Céolin[*,¶]

†*Sorbonne Université, CNRS, Laboratoire de Chimie Physique Matière et Rayonnement, UMR 7614, F-75005 Paris, France*

‡*Theoretische Chemie, Physikalisch-Chemisches Institut, Universität Heidelberg, Im Neuenheimer Feld 229, D-69120 Heidelberg, Germany*

¶*Synchrotron SOLEIL, l'Orme des Merisiers, Saint-Aubin, F-91192 Gif-sur-Yvette Cedex, France*

§*Faculty of Science, Nakhon Phanom University, Nakhon Phanom 48000, Thailand*

‖*School of Physics, Suranaree University of Technology, Nakhon Ratchasima 30000, Thailand*

⊥*Department of Applied Physics, Faculty of Sciences and Liberal Arts, Rajamangala University of Technology Isan, Nakhon Ratchasima 30000, Thailand*

#*Interdisciplinary Center for Scientific Computing, Ruprecht-Karls University, Im Neuenheimer Feld 205A, D-69120 Heidelberg, Germany*

@*MAX IV Laboratory, Lund University, P.O. Box 118, SE-22100 Lund, Sweden*

△*Fachbereich Physik, Freie Universität Berlin, Arnimallee 14, D-14195, Berlin, Germany*

E-mail: tsveta.miteva@upmc.fr; denis.ceolin@synchrotron-soleil.fr

Methods

Experimental

For the present experiment we used the newly operational microjet setup that was specifically designed for the HAXPES station of the GALAXIES beamline[1,2]. A differentially-pumped tube in which the microjet head is inserted, is mounted on a 3-axes motorized manipulator in front of the spectrometer lens. Two holes of 2 mm diameter allow the photons to go in and out. At the end of the tube and in front of the lens, a 500 μm diameter hole skimmer allows the electrons created at the interaction point to go in the direction of the spectrometer. The microjet head is mostly composed of a 30 μm diameter vertical glass capillary facing a temperature-controlled catcher in CuBe having a 300 μm hole, and a camera. Piezo motors allow their precise alignment relative to each other and to the photon beam. The catcher is placed at a distance of about 5 mm from the capillary and is permanently pumped in order to extract the liquid. For the present experiment, a 0.5M KCl aqueous solution is injected in the capillary by a high performance liquid chromatography (HPLC) pump with a constant flux of 1.6 ml/min. The alignment of the setup is performed on the KCl aqueous solution by measuring the water O1s x-ray photoelectron peak intensity and by optimizing the liquid vs gas phase ratio. The pressure in the main chamber is kept below the 10^{-5} mbar range whereas it is kept at about 10^{-4} mbar in the differentially-pumped tube when the HPLC pump is ON. Our equipment is an updated version of the equipment used in Ref.[3] The aqueous potassium chloride solution was prepared by mixing >99% KCl salt with deionized water. Filtering and degazing procedures were systematically performed before injecting the solution. The spectrometer resolution of about 0.6 eV was achieved with the 500 eV pass energy and 0.5 mm slits. The photon energy resolution achieved at 2.8 keV and 3.6 keV was about 0.3 eV and 0.4 eV, respectively. The experimental 2D maps representing the evolution of the KLL Auger spectra in the vicinity of the Cl^- and K^+ K-edges, as a function of the photon energy, are shown in Figs. 2 and 3 in the main text, respectively. The aqueous

K^+ and Cl^- 1s ionization potentials were measured at $h\nu = 5\,keV$ and calibrated on the liquid contribution of the O1s XPS spectrum.[4] The maps were also calibrated using the O1s photoelectron line of liquid water but at photon energies close to the potassium and chloride 1s ionization thresholds.

Ab initio calculations

The theoretical X-ray absorption spectra were computed for the hexa-coordinated clusters $K^+(H_2O)_6$ and $Cl^-(H_2O)_6$, which can be considered as representatives of the complete first solvation shell of the two ions K^+ and Cl^- [5–7]. The two structures shown in Fig. 4 of the main text were optimized at the DFT level of theory using the B3LYP functional and the 6-311++G(2d,2p) basis set[8,9]. The geometry optimization was performed with the Gaussian 09 package[10]. In order to obtain a realistic structure for K^+ corresponding to the bulk solution, we carried out constrained geometry optimization by choosing the equilibrium gas-phase geometries[11,12] belonging to the D_3 point group and then increasing the angle θ between the K-O bond and the C_3 axis to 55°. This angle was chosen such that the O-K-O angles are around the maxima of the angular distributions obtained from quantum mechanics/molecular mechanics simulations reported in Ref.[7]. Moreover, we fixed the K-O distance to 2.840 Å, in agreement with the values obtained other theoretical and experimental works[5–7].

The energies and transition moments of the core-excited states of the isolated ions and microsolvated clusters were computed with the algebraic diagrammatic construction method for the polarization propagator[13] within the core-valence separation approximation[14–16] (CVS-ADC(2)x) as implemented in the Q-Chem package[17–20]. In the case of Cl^- the 6-311++G(3df,3pd) basis set[8,21] (excluding f functions) was used on all atoms, whereas in the case of K^+ we used the 6-311+G(2d,p) basis set[8,9] on all atoms, and two additional sets of s, p and d diffuse functions were added on K. The use of a smaller basis set in the case of K is due to the higher number of atomic orbitals compared to the case of Cl, and therefore, prohibitively high cost of the CVS-ADC(2)x computation. In our calculations the core

space comprises the 1s orbital of K^+ or Cl^-, whereas the remaining occupied orbitals are included in the valence space. For the calculations of the XAS spectra we used the C_2 point group in the case of $K^+(H_2O)_6$ and $Cl^-(H_2O)_6$. To account for the lifetime broadening due to the Auger decay of the core-excited states, we convolved the theoretical spectra with a Lorentzian function of FWHM 0.74 eV and 0.62 eV in the case of K^+ and Cl^-, respectively[22]. Additionally, we convolved the theoretical spectra with a Gaussian profile to also account for the experimental resolution (see Fig. 4 in the main text). We analyzed the core-excited states by expanding the natural orbitals occupied by the excited electron (singly occupied natural orbitals, SONOs) ψ_i of the microsolvated clusters in the basis of SONOs of the bare K^+ or Cl^- ions, χ_{nl}

$$\psi_i = \sum_{nl} a^i_{nl} \chi_{nl} \tag{1}$$

where n and l stand for the principal and orbital quantum numbers as described in Ref.[23]. The expansion coefficients a^i_{nl} show the degree of delocalization of the excited electron and the mixing of the core-excited states in the ligand field created by the surrounding water molecules (see Fig. 4).

The $2p^{-2}nl$ final states following KLL resonant Auger decay of $K^+(H_2O)_6$ and $Cl^-(H_2O)_6$ were computed at the Configuration Interaction Singles (CIS) level using the Graphical Unitary Group Approach (GUGA) as implemented in the GAMESS-US package[24–26]. In order to account for the relaxation effects upon core ionization, we employed a restricted open-shell Hartree-Fock reference wave function with a hole in the 2s orbital of both K^+ and Cl^-. We used the 6-311++G(2d,2p) basis set[8,9,21] on all atoms. Additionally, the basis set was augmented with two sets of s, p, d diffuse functions in the case of K^+, and three sets of s, p, d diffuse functions in the case of Cl^-. The larger basis set employed in the case of Cl was necessary in order to ensure the convergence of the excited states. The active space comprises the 2s and 2p orbitals of K/Cl with occupancy fixed to 6 and all virtual orbitals with occupancy fixed to 1. The remaining doubly occupied orbitals were frozen in the calculation.[27]

PCI shift

The maximum amplitude of the PCI shift is estimated by comparing the positions of the normal KLL Auger lines of both Cl^-_{aq} and K^+_{aq} close to threshold with those recorded far from threshold, at photon energies $h\nu = 5\,keV$[28]. In this way, we found for the present spectra a shift of $\sim$1 eV of the maxima towards higher kinetic energies as compared to the spectra reported in[28]. The magnitude of the shift is similar for the two ions and constant in the photon energy range of up to about 8 eV above threshold. The PCI shift of isoelectronic atom argon in the gas phase show also a maximum value of 1 eV, however, it decreases in the first 8 eV above threshold by approximately 0.6 eV[29]. A possible explanation of the shift observed in our experiment is given in Ref.[30] where it was proposed that it is due to a process of internal ionization, i.e. excitation of the photoelectron into the conduction band, followed by normal Auger decay. The observed shift was explained as resulting from the PCI-like interaction between the Auger electron and the electron excited to the conduction band.

Core-excited states of Cl^-

In the calculated spectrum of Cl^- the intensity of the $Cl^-(1s^{-1}4p)$ state is lower than that of the $Cl^-(1s^{-1}5p)$ state, contrary to what is observed in K^+. This difference can be explained by the lower electron density of the 4p compared to the 5p electron in the region close to the core hole which thus results in the lower oscillator strength of the $1s^{-1}4p$ compared to the $1s^{-1}5p$ transition in Cl^- (see Fig. 1 in SI). In what follows we give a simple explanation of the difference in the radial density distributions of the $1s^{-1}4p$ and $1s^{-1}5p$ states in K^+ and Cl^-. In the case of K^+, the excited electron mainly sees a $2/r$ potential. In addition, it sees a short range potential originating from the point-like nucleus and the screening electrons. The influence of the latter can be described by a quantum defect $\delta \neq 0$, which is almost constant for the entire infinite Rydberg series. However, in case of Cl^- the outer electron does not experience a Coulomb potential and the short range potential becomes dominant. As a result

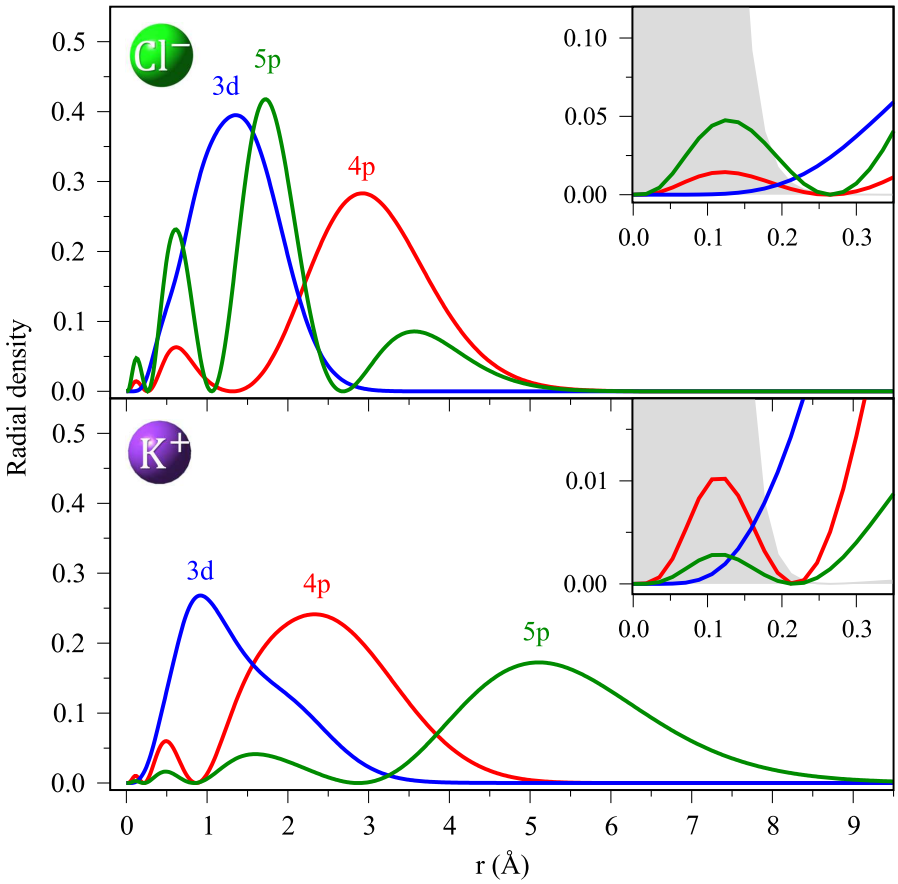

Figure SI 1: Radial density distributions of the singly-occupied natural orbital occupied by the excited electron corresponding to the $1s^{-1}4p$, $1s^{-1}3d$ and $1s^{-1}5p$ core excitations in K^+ (lower panel) and Cl^- (upper panel). The insets show the region of distances relevant for the overlap with the 1s core orbital whose radial density is shown as a grey shaded area.

of the absence of the Coulomb potential we see a different behavior in the properties of the states, like e.g. only a finite number of bound states, the $1s^{-1}4p$ state in the case of Cl^- [31]. In contrast to this, the $1s^{-1}3d$ and $1s^{-1}5p$ states are not bound.

Delocalization vs resonant Auger decay

In order to estimate the delocalization rate of the core-excited electron at the pre-edges of K^+ and Cl^-, we used the core-hole clock method.[32–36] In the case of Cl^-, it was possible to perform the same data treatment as in Ref.[37] i.e., for each photon energy step, all components of the 2D map shown in Fig. 3(a) of the main text were isolated by fitting procedures and

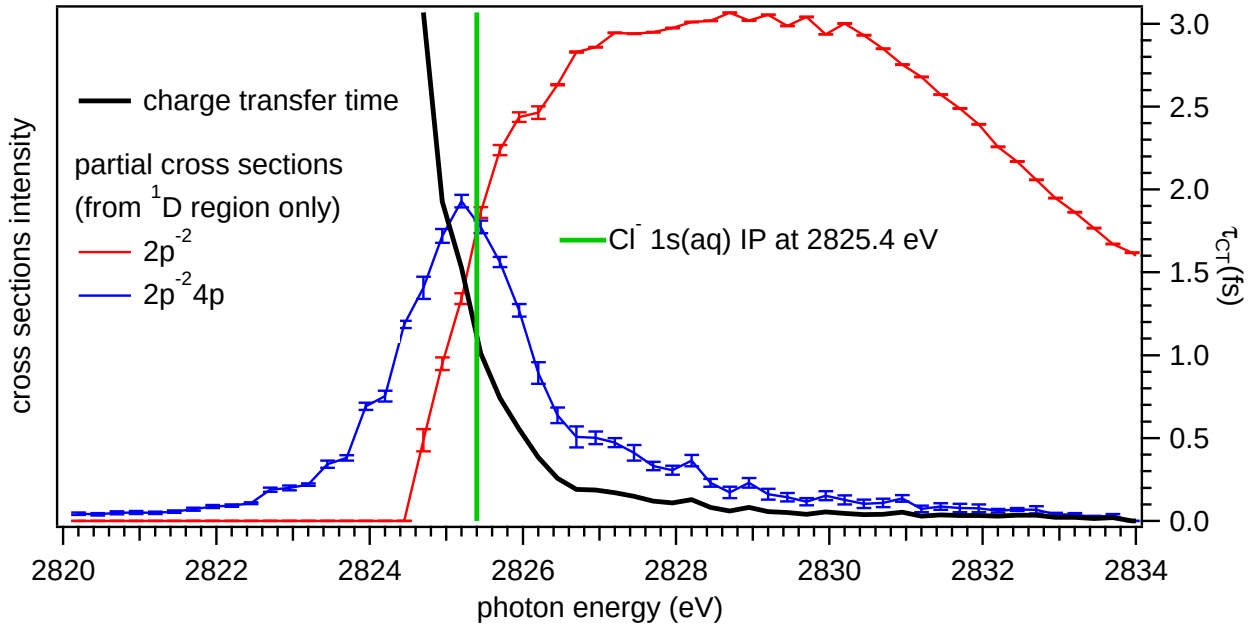

Figure SI 2: Partial cross sections and charge transfer time extracted from Fig. 3. The blue and red curves are obtained by integrating the area of the $2p^{-2}$ and $2p^{-2}4p$ final states (^{1}D state region only) at each photon energy step. From these curves we determine the charge transfer time τ_{CT} according to the formula $\tau_{\mathrm{CT}} = \tau_c l/d$, with τ_c being the Cl 1s core-hole lifetime and l/d being the intensity ratio of the localized ($2p^{-2}4p$) and delocalized ($2p^{-2}$) states at a given excitation energy.[32] The green line defines the $Cl^-_{aq}(1s)$ ionization potential.

their intensity integrated to get the partial electron yield as a function of the photon energy. The result is presented on Fig. 2 in the SI. The figure shows that there is a large overlap between the resonant and normal Auger contributions, due to the proximity of the resonance to the ionization potential and due to the very short lifetime of the corresponding states. At the specific photon energy of hν = 2825.2 eV, i.e. at the maximum of the lowest core excitation $1s^{-1}4p$, the resonant Auger spectrum exhibits a double-peak structure in the interval E_{kin} = 2380 − 2385 eV (Fig. 3(c) of main text). The position of the first peak coincides with the ^{1}D main line resulting from normal Auger decay, whereas the second peak at 2383.5 eV corresponds to the resonant Auger decay to the $2p^{-2}(^1D)4p$ states. By fitting this double-peak structure with two Voigt functions, we determine the intensity ratio l/d of the localized ($2p^{-2}4p$) and the delocalized ($2p^{-2}$) decay products at a given excitation energy. From this ratio and the Auger lifetime τ_c, one can determine the photon-energy dependent delocalization time τ_{CT} according to the relation $\tau_{CT} = \tau_c l/d$[32–36]. Close to the maximum of the $1s^{-1}4p$ resonance the ratio $l/d \cong 1$ and, as a consequence, the delocalization time τ_{CT} is of the same order as the Auger lifetime, i.e. ∼1 fs. The fast delocalization in this case is a result of the fact that the energy splitting between the Cl^- ($1s^{-1}4p$) resonance and the ionization threshold is 0.2 eV, and thus, smaller than the lifetime broadening of 0.62 eV[28].

For potassium, a comparable data treatment is more complicated due to the presence of multiple simultaneous processes, namely, normal and resonant Auger decay, as well as charge transfer from solvent. To extract the intensity of each component from the 2D map shown in Fig. 2(a) of the main text, one needs the spectral fingerprints of each process to be separated. However, as can be seen, this is hardly possible especially close to threshold in the kinetic energy region 2965 – 2970 eV. For instance, at hν = 3610.7 eV on the high kinetic-energy side of the ^{1}D main line, there are contributions from the PCI tail and from the $2p^{-2}(^1D)4p$ resonant Auger state. On the low kinetic energy side, the charge transfer processes lead to a very large structure whose shape unfortunately cannot be easily simulated based on known profiles. The lifetime of the 1s core hole is shorter for potassium than for chloride (0.9 vs. 1 fs)

and, moreover, the core-excited state appears 1.2 eV below the ionization threshold whereas it is only 0.2 eV for chloride. Therefore, one can expect much less efficient delocalization in K^+_{aq} compared to Cl^-_{aq}.

References

(1) Céolin, D.; Ablett, J.; Prieur, D.; Moreno, T.; Rueff, J.-P.; Marchenko, T.; Journel, L.; Guillemin, R.; Pilette, B.; Marin, T. et al. Hard X-ray photoelectron spectroscopy on the GALAXIES beamline at the SOLEIL synchrotron. *J. Electron Spectrosc. Relat. Phenom.* **2013**, *190, Part B*, 188 – 192.

(2) Rueff, J.-P.; Ablett, J. M.; Céolin, D.; Prieur, D.; Moreno, T.; Balédent, V.; Lassalle-Kaiser, B.; Rault, J. E.; Simon, M.; Shukla, A. The GALAXIES beamline at the SOLEIL synchrotron: inelastic X-ray scattering and photoelectron spectroscopy in the hard X-ray range. *J. Synchrotron Rad.* **2015**, *22*, 175–179.

(3) Faubel, M.; Schlemmer, S.; Toennies, J. P. A molecular beam study of the evaporation of water from a liquid jet. *Z. Phys. D* **1988**, *10*, 269–277.

(4) Winter, B.; Faubel, M. Photoemission from Liquid Aqueous Solutions. *Chem. Rev.* **2006**, *106*, 1176–1211, PMID: 16608177.

(5) Ohtaki, H.; Radnai, T. Structure and dynamics of hydrated ions. *Chem. Rev.* **1993**, *93*, 1157–1204.

(6) Soper, A. K.; Weckström, K. Ion solvation and water structure in potassium halide aqueous solutions. *Biophys. Chem.* **2006**, *124*, 180 – 191.

(7) Ma, H. Hydration structure of Na^+, K^+, F^-, and Cl^- in ambient and supercritical water: A quantum mechanics/molecular mechanics study. *Int. J. Quant. Chem.* **2014**, *114*, 1006–1011.

(8) Krishnan, R.; Binkley, J. S.; Seeger, R.; Pople, J. A. SelfâĂŘconsistent molecular orbital methods. XX. A basis set for correlated wave functions. *J. Chem. Phys.* **1980**, *72*, 650–654.

(9) Blaudeau, J.-P.; McGrath, M. P.; Curtiss, L. A.; Radom, L. Extension of Gaussian-2 (G2) theory to molecules containing third-row atoms K and Ca. *J. Chem. Phys.* **1997**, *107*, 5016–5021.

(10) Frisch, M. J.; Trucks, G. W.; Schlegel, H. B.; Scuseria, G. E.; Robb, M. A.; Cheeseman, J. R.; Scalmani, G.; Barone, V.; Mennucci, B.; Petersson, G. A. et al. Gaussian 09 Revision D.01. Gaussian Inc. Wallingford CT 2009.

(11) Lee, H. M.; Kim, J.; Lee, S.; Mhin, B. J.; Kim, K. S. Aqua-potassium(I) complexes: Ab initio study. *J. Chem. Phys.* **1999**, *111*, 3995–4004.

(12) Lee, H. M.; Kim, D.; Kim, K. S. Structures, spectra, and electronic properties of halide-water pentamers and hexamers, $X^-(H_2O)_{5,6}$ (X=F,Cl,Br,I): Ab initio study. *J. Chem. Phys.* **2002**, *116*, 5509–5520.

(13) Schirmer, J. Beyond the random-phase approximation: A new approximation scheme for the polarization propagator. *Phys. Rev. A* **1982**, *26*, 2395–2416.

(14) Barth, A.; Schirmer, J. Theoretical core-level excitation spectra of N_2 and CO by a new polarisation propagator method. *J. Phys. B At. Mol. Opt. Phys.* **1985**, *18*, 867.

(15) Cederbaum, L. S.; Domcke, W.; Schirmer, J. Many-body theory of core holes. *Phys. Rev. A* **1980**, *22*, 206–222.

(16) Barth, A.; Cederbaum, L. S. Many-body theory of core-valence excitations. *Phys. Rev. A* **1981**, *23*, 1038–1061.

(17) Wenzel, J.; Wormit, M.; Dreuw, A. Calculating core-level excitations and x-ray absorption spectra of medium-sized closed-shell molecules with the algebraic-diagrammatic

construction scheme for the polarization propagator. *J. Comp. Chem.* **2014**, *35*, 1900–1915.

(18) Wenzel, J.; Wormit, M.; Dreuw, A. Calculating X-ray Absorption Spectra of Open-Shell Molecules with the Unrestricted Algebraic-Diagrammatic Construction Scheme for the Polarization Propagator. *J. Chem. Theory Comput.* **2014**, *10*, 4583–4598.

(19) Wormit, M.; Rehn, D. R.; Harbach, P. H.; Wenzel, J.; Krauter, C. M.; Epifanovsky, E.; Dreuw, A. Investigating excited electronic states using the algebraic diagrammatic construction (ADC) approach of the polarisation propagator. *Mol. Phys.* **2014**, *112*, 774–784.

(20) Shao, Y.; Gan, Z.; Epifanovsky, E.; Gilbert, A. T.; Wormit, M.; Kussmann, J.; Lange, A. W.; Behn, A.; Deng, J.; Feng, X. et al. Advances in molecular quantum chemistry contained in the Q-Chem 4 program package. *Mol. Phys.* **2015**, *113*, 184–215.

(21) McLean, A. D.; Chandler, G. S. Contracted Gaussian basis sets for molecular calculations. I. Second row atoms, Z=11âĂŞ18. *J. Chem. Phys.* **1980**, *72*, 5639–5648.

(22) Krause, M. O.; Oliver, J. H. Natural widths of atomic K and L levels, Kα X-ray lines and several KLL Auger lines. *J. Phys. Chem. Ref. Data* **1979**, *8*, 329–338.

(23) Miteva, T.; Wenzel, J.; Klaiman, S.; Dreuw, A.; Gokhberg, K. X-Ray absorption spectra of microsolvated metal cations. *Phys. Chem. Chem. Phys.* **2016**, *18*, 16671–16681.

(24) Brooks, B. R.; Laidig, W. D.; Saxe, P.; Handy, N. C.; Schaefer III, H. F. The Loop-Driven Graphical Unitary Group Approach: A Powerful Method for the Variational Description of Electron Correlation. *Phys. Scr.* **1980**, *21*, 312.

(25) Brooks, B. R.; Schaefer, H. F. The graphical unitary group approach to the electron

correlation problem. Methods and preliminary applications. *J. Chem. Phys.* **1979**, *70*, 5092–5106.

(26) Schmidt, M. W.; Baldridge, K. K.; Boatz, J. A.; Elbert, S. T.; Gordon, M. S.; Jensen, J. H.; Koseki, S.; Matsunaga, N.; Nguyen, K. A.; Su, S. et al. General atomic and molecular electronic structure system. *J. Comp. Chem.* **1993**, *14*, 1347–1363.

(27) Mosnier, J.-P.; Kennedy, E. T.; van Kampen, P.; Cubaynes, D.; Guilbaud, S.; Sisourat, N.; Puglisi, A.; Carniato, S.; Bizau, J.-M. Inner-shell photoexcitations as probes of the molecular ions CH^+, OH^+, and SiH^+: Measurements and theory. *Phys. Rev. A* **2016**, *93*, 061401.

(28) Céolin, D.; Kryzhevoi, N. V.; Nicolas, C.; Pokapanich, W.; Choksakulporn, S.; Songsiriritthigul, P.; Saisopa, T.; Rattanachai, Y.; Utsumi, Y.; Palaudoux, J. et al. Ultrafast Charge Transfer Processes Accompanying KLL Auger Decay in Aqueous KCl Solution. *Phys. Rev. Lett.* **2017**, *119*, 263003.

(29) Guillemin, R.; Sheinerman, S.; Püttner, R.; Marchenko, T.; Goldsztejn, G.; Journel, L.; Kushawaha, R. K.; Céolin, D.; Piancastelli, M. N.; Simon, M. Postcollision interaction effects in KLL Auger spectra following argon $1s$ photoionization. *Phys. Rev. A* **2015**, *92*, 012503.

(30) Tchaplyguine, M.; Kivimäki, A.; Peredkov, S.; Sorensen, S. L.; Öhrwall, G.; Schulz, J.; Lundwall, M.; Rander, T.; Lindblad, A.; Rosso, A. et al. Localized versus delocalized excitations just above the 3d threshold in krypton clusters studied by Auger electron spectroscopy. *J. Chem. Phys.* **2007**, *127*, 124314.

(31) Buckman, S. J.; Clark, C. W. Atomic negative-ion resonances. *Rev. Mod. Phys.* **1994**, *66*, 539–655.

(32) Föhlisch, A.; Feulner, P.; Hennies, F.; Fink, A.; Menzel, D.; Sanchez-Portal, D.;

Echenique, P. M.; Wurth, W. Direct observation of electron dynamics in the attosecond domain. *Nature* **2005**, *436*, 373.

(33) Björneholm, O.; Nilsson, A.; Sandell, A.; Hernnäs, B.; Mrtensson, N. Determination of time scales for charge-transfer screening in physisorbed molecules. *Phys. Rev. Lett.* **1992**, *68*, 1892–1895.

(34) Karis, O.; Nilsson, A.; Weinelt, M.; Wiell, T.; Puglia, C.; Wassdahl, N.; Mårtensson, N.; Samant, M.; Stöhr, J. One-Step and Two-Step Description of Deexcitation Processes in Weakly Interacting Systems. *Phys. Rev. Lett.* **1996**, *76*, 1380–1383.

(35) Wurth, W.; Menzel, D. Ultrafast electron dynamics at surfaces probed by resonant Auger spectroscopy. *Chem. Phys.* **2000**, *251*, 141 – 149.

(36) Brühwiler, P. A.; Karis, O.; Mårtensson, N. Charge-transfer dynamics studied using resonant core spectroscopies. *Rev. Mod. Phys.* **2002**, *74*, 703–740.

(37) Céolin, D.; Marchenko, T.; Guillemin, R.; Journel, L.; Kushawaha, R. K.; Carniato, S.; Huttula, S.-M.; Rueff, J. P.; Armen, G. B.; Piancastelli, M. N. et al. Auger resonant-Raman study at the Ar K edge as probe of electronic-state-lifetime interferences. *Phys. Rev. A* **2015**, *91*, 022502.